All-Optical Ultrafast Switching in 2 × 2 Silicon Microring Resonators and its Application to Reconfigurable DEMUX/MUX and Reversible Logic Gates

Purnima Sethi, *Student Member, IEEE*, and Sukhdev Roy, *Senior Member, IEEE*

Abstract—We present a theoretical model to analyze all-optical switching by two-photon absorption induced free-carrier injection in silicon 2 × 2 add-drop microring resonators. The theoretical simulations are in good agreement with experimental results. The results have been used to design all-optical ultrafast (i) reconfigurable De-multiplexer/Multiplexer logic circuits using three microring resonator switches and (ii) universal, conservative and reversible Fredkin and Toffoli logic gates with only one and two microring resonator switches respectively. Switching has been optimized for low-power (25 mW) ultrafast (25 ps) operation with high modulation depth (85%) to enable logic operations at 40 Gb/s. The combined advantages of high Q-factor, tunability, compactness, cascadability, reversibility and reconfigurability make the designs favorable for practical applications. The proposed designs provide a new paradigm for ultrafast CMOS-compatible all-optical reversible computing circuits in silicon.

Index Terms—Coupled mode analysis, integrated optics, optical computing, optical logic devices, optical resonators, optical switches, silicon, switching circuits, ultrafast optics.

I. Introduction

SILICON holds tremendous potential to meet the anticipated future requirements for ultrafast and ultrahigh bandwidth communication and computing. Silicon photonics exploits the advantages of optics i.e. parallelism, ultrafast speed and ultrahigh bandwidth, along with CMOS compatibility, to overcome the challenges faced by electronics, enabling ultra-compact footprint in addition to energy efficiency [1]–[4]. Advances in the fabrication of microstructures especially microring resonators (MRRs) have facilitated strong optical confinement that can lead to energy-efficient optical computing [4], [5]. A switch is the basic building block of computing circuits. Silicon ring resonators provide a very versatile platform for optical switching and computing, offering advantages of high-Q, ultrafast and ultralow-power switching, ease of fabrication and large-scale integration [4]–[14].

Silicon ring resonators based optical switches modulated by electrical [6], thermal [7], or optical [8]–[12] signals have been widely investigated. There is a tremendous impetus for realization of all-optical ultrafast and ultrahigh bandwidth computing devices and circuits in silicon with simple designs to circumvent cumbersome and power consuming optoelectronic conversions.

The need for power optimization along with faster computing requires novel computing paradigms [6], [7], [13]–[21]. Reconfigurability offers adaptability, wherein the same circuit can be reconfigured and dynamically tailored to perform various application specific operations and help in reducing cost, size and power consumption to make flexible and upgradable systems [13]. Binary decision diagram (BDD) and directed logic (DL) are recent computing strategies which employ an optical switching network to perform complicated logic functions by taking advantage of fast and low-loss propagation of light [6], [7], [14]. Although, BDD and DL minimize latency, designs of circuits based on conventional classical Boolean logic lead to information loss and energy dissipation. This limitation can be overcome by conservative and reversible logic that circumvents information loss and opens up the possibility of ultra-low power computing [15]–[21]. Reversible logic is also quintessential to enable revolutionary optical and quantum computing paradigms. Fredkin and Toffoli are fundamental, conservative, reversible and universal logic gates for quantum computing. Unlike many quantum gates, these gates have a classical analog and are building blocks for importing complex classical operations into quantum algorithms and simulations [21]. They also play an important role in phase estimation, error correction and fault tolerant quantum circuits [19]–[21].

All-optical switching in silicon MRRs based on free-carrier injection by two-photon absorption (TPA) has been experimentally shown in both all-pass (1 × 1) and add-drop (1 × 2) configurations [8]–[11]. All-optical AND/NAND and half-adder/full-adder circuits have been experimentally realized using 1 × 1 MRRs only [8]–[12]. Extensive efforts have been directed towards the implementation of BDD and DL based computing circuits with silicon MRRs using electro and thermo-optic modulation, although they suffer from lower switching times (∼ms-ns) [6], [7]. Xu and Soref have proposed a reconfigurable electro-optic DL architecture to realize full-adder, De-multiplexer/Multiplexer (DEMUX/MUX), encoder and

comparator, by rewiring arrays of hundreds of 1×1 silicon switches controlled by the logic input signals [6]. However, the above designs require large number of switches for realization of the desired logic. Reduction in the number of switches can substantially reduce power consumption, delay, latency and size of the devices. To the best of our knowledge, 1×2 and 2×2 MRR configurations have not been used so far to design all-optical computing circuits in silicon.

All-optical switching through TPA induced carrier injection has been theoretically analyzed in all-pass (1×1) MRRs using coupled-mode theory in which the dynamics were simulated in terms of temporal variation of optical and material properties [22]. A simple model has also been proposed to analyze the dynamics of a 1×2 MRR configuration that neglects scattering losses and linear and non-linear effects [23]. However, a more accurate model needs to be developed for a rigorous analysis of all-optical switching in 1×2 and 2×2 MRRs. The add-drop MRR configuration is a versatile switching configuration that can form the template for high-density integration of micro-photonic devices for routing, filtering, modulation and lasing and are envisaged to be the building blocks for optical dispersion compensators, delay lines, optical sensors, optical time division multiplexed, wavelength division multiplexed and space division multiplexed systems [4].

Recently, all-optical switching in an optically controlled 1×2 MRR has been demonstrated with bacteriorhodopsin (BR) protein-coated silica microcavities in contact between two tapered single-mode fibers at telecom wavelengths, which has also been used to design higher computing circuits and reversible logic gates [13], [24]–[26]. However, the prototype with switching time $\sim \mu s$ presently limits its applicability for high bit rates. Although a few physical implementations of reversible Fredkin and Toffoli logic gates with resonant structures have been shown, all-optical reversible logic has not yet been realized using silicon MRRs [15], [16], [20]. Hence, BDD/DL based reversible all-optical computing logic using silicon MRRs holds tremendous potential for realization of low-cost large scale integrated CMOS-photonic chips.

Thus, the objective of this paper is (i) to develop an accurate theoretical model to analyze all-optical switching in a 2×2 add-drop silicon MRR through carrier injection by TPA using coupled-mode theory and to optimize it to design ultrafast (ii) reconfigurable DEMUX/MUX and (iii) universal, conservative and reversible Fredkin and Toffoli logic gates.

II. THEORETICAL MODEL

We consider an all-optical switch in a 2×2 add-drop silicon ring resonator configuration as shown in Fig. 1. Here, the input ports are labeled P_i (input) and P_a (add) and output ports as P_t (through) and P_d (drop) respectively. Prior to the arrival of pump pulse, the probe pulse is in high transmission at P_t. However, the pump pulse generates free carriers inside the MRR due to TPA which reduces the refractive index of silicon through plasma-dispersion effect. This changes the resonance wavelength of the resonator, which couples the probe into the MRR, yielding a high transmission at P_d and low transmission at P_t. After
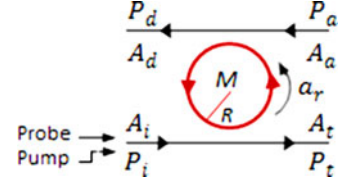

Fig. 1. Schematic of an all-optical 2×2 add-drop MRR switch.

the passage of the control pulse, the resonant wavelength and transmission of probe relax back due to fast recombination of the carriers determined by the carrier recombination lifetime in the MRR.

The switching response of the silicon add-drop MRR can be modeled considering the propagation of pump and probe using time-domain coupled-mode theory [22], [27]. We consider A_i and A_a as the input field amplitudes at P_i and P_a respectively and A_t and A_d as the output field amplitudes at P_t and P_d respectively. The ring is considered as a lumped oscillator where, $|A_x|^2$ ($x = i, a, t, d$) is the power of the waveguide mode and supports a travelling wave of amplitude $A_r (A_i \neq 0, A_a = 0)$, which is normalized so that $|A_r|^2$ represents the total power flowing through the cross-section A of the ring waveguide at time t. The total energy stored in the ring is $|a_r|^2$ with energy amplitude a_r, which decays at the total rate $r = \tau^{-1} = r_o + r_e + r_d, r_o = \frac{\alpha_o v_g}{2}$ is the decay rate due to intrinsic effects such as absorption and surface scattering, $r_e = \frac{\mu_e^2}{2} = \frac{\kappa_e^2 v_g}{2L}$ is the decay rate due to external coupling with the input waveguide and $r_d = \frac{\mu_d^2}{2} = \frac{\kappa_d^2 v_g}{2L}$ is the energy decay rate due to external coupling between the ring and drop waveguide, where τ is total decay time constant, v_g is group velocity and μ_e, μ_d and κ_e, κ_d are the corresponding mutual and power coupling coefficients respectively. The relation between a_r and A_r is given by $|a_r|^2 = \frac{2\pi R}{v_g} |A_r|^2$ where $L = 2\pi R$ is the round-trip length of the cavity. Considering ω_o as the resonant frequency of the MRR, the rate of change in energy is given by [27]

$$\frac{da_r}{dt} = \left(j\omega_o - \frac{1}{\tau} \right) a_r - j\mu_e A_i \qquad (1)$$

For small round-trip loss, weak coupling and frequencies $\omega - \omega_o \ll \omega_o$, the field amplitude coupled into the MRR waveguide can be written as [27], [28]

$$a_r = \frac{-j\sqrt{2r_e}}{j(\omega - \omega_o) + r} A_i. \qquad (2)$$

The output field amplitude in the waveguide is given by

$$A_t(t) = A_i(t) - j\sqrt{2r_e} a_r(t) \qquad (3)$$

$$A_d(t) = -j\sqrt{2r_d} a_r(t). \qquad (4)$$

The transmission response of the MRR at P_t and P_d respectively is given by,

$$T(\omega) = \frac{A_t}{A_i} = \frac{j(\omega - \omega_o) + r - 2r_e}{j(\omega - \omega_o) + r},$$

$$D(\omega) = \frac{A_d}{A_i} = \frac{-2\sqrt{r_e r_d}}{j(\omega - \omega_o) + r}. \qquad (5)$$

The complex resonance frequency is defined as $\tilde{\omega}_o = \omega_o + jr_o$. The decay rate can also be written as, $r = \frac{\omega_o}{2Q_o} + \frac{\omega_o}{2Q_e} + \frac{\omega_o}{2Q_d}$, where Q_o, Q_e and Q_d are the corresponding quality factors. The critical coupling condition where all signal power is extracted by the resonator at resonance is $r_e = r_d + r_o$ and the optimal coupling condition (for maximum drop port transmission) is $r_e = r_d = (r - r_o)/2$ [27], [28]. For ultrafast switching, free-carrier plasma-dispersion effect is used to modulate the refractive index of silicon. When a strong optical pump and a weak continuous (*cw*) probe are coupled into the MRR through two different resonances, the pump generates free carriers in MRR due to TPA. The generated free carriers reduce the refractive index of silicon and blue-shift the ring resonances. The electric field in the ring waveguide can be written as $\vec{E} = a_r \overrightarrow{e}(x, y) e^{-j\tilde{\beta}z}$, with energy normalization, $\frac{1}{2}\varepsilon_o \iiint n^2 |\vec{E}|^2 dxdydz = |a_r|^2$, where $\tilde{\beta}$ is the complex propagation constant. It can be assumed that $\iiint dxdydz \approx L \iint dxdy$, where z is defined along the ring circumference and x and y in the cross-section of the ring waveguide. The real and the imaginary part of the resonance frequency shift (energy decay rate change) respectively can be written as,

$$\Delta\omega_o^L = -\omega_o \Gamma \frac{\Delta n}{n_r} \text{ and } \Delta r_o^L = \Gamma \frac{c\Delta\alpha}{2n_r} \tag{6}$$

Where n_r is the refractive index of ring waveguide core and Γ is confinement factor. The induced real refractive index and optical absorption coefficient variations (Δn and $\Delta\alpha$) at 1.55 μm are given by [22]

$$\Delta n = \Delta n_e + \Delta n_h =$$
$$- \left[8.8 \times 10^{-22} \Delta N_e + 8.5 \times 10^{-18} (\Delta N_h)^{0.8} \right] \tag{7a}$$

$$\Delta\alpha = \Delta\alpha_e + \Delta\alpha_h =$$
$$\left[8.5 \times 10^{-18} \Delta N_e + 6 \times 10^{-18} (\Delta N_h) \right]. \tag{7b}$$

Δn_e and Δn_h are the refractive-index changes due to change in electron concentration $\Delta N_e (cm^{-3})$ and hole concentration $\Delta N_h (cm^{-3})$ respectively, whereas $\Delta\alpha_e (cm^{-1})$ and $\Delta\alpha_h (cm^{-1})$ are the corresponding absorption coefficient variations respectively. This effect also causes small nonlinear index and absorption changes due to Kerr effect which are given by, $\Delta n^{NL} = n_{21} I_{\text{pump}}$ and $\Delta\alpha^{NL} = \beta I_{\text{pump}}$, where n_{21} and β are the Kerr and TPA coefficients respectively. The input pump intensity coupled into MRR is $I_{\text{pump}} = \frac{1}{2}c\varepsilon_o n |\overrightarrow{E_{\text{pump}}}|^2$. Assuming that refractive index of core is uniform; the nonlinear changes can be expressed as,

$$\Delta\omega_o^{NL} = -\omega_o \frac{cn_{21}}{n_r^2} \frac{|a_r^{\text{pump}}|^2}{V_{\text{eff}}} \text{ and}$$

$$\Delta r_o^{NL} = \beta \frac{c^2}{2n_r^2} \frac{|a_r^{\text{pump}}|^2}{V_{\text{eff}}}. \tag{8}$$

Here, $V_{\text{eff}} = LA_{\text{eff}}$, is the effective volume of the MRR and A_{eff} is the effective area. The red-shift caused by the Kerr effect is smaller than the blue-shift, due to which the latter effect dominates in silicon MRR. The output power of the probe then gets modulated by the resonance shift. The free carrier concentration change ($\Delta N_e = \Delta N_h = \Delta N$) generated primarily by TPA is given by $\frac{dN(t)}{dt} = \frac{\beta I_{\text{pump}}^2}{2h\nu} - \frac{N(t)}{\tau_{fc}}$, which can be written as,

$$\frac{dN(t)}{dt} = \frac{\Delta r_o^{NL}}{\hbar\omega_{\text{pump}}} \frac{|a_r^{\text{pump}}|^2}{V} - \frac{N(t)}{\tau_{fc}} \tag{9}$$

where, $\hbar\omega_{\text{pump}}$ is the pump photon energy and τ_{fc} is the free carrier recombination lifetime.

In order to analyze the dynamic behavior of the switching mechanism, low-loss ring resonators are considered so that the spatial variation of the fields along the ring circumference can be neglected and only temporal variation is taken into account. The nonlinear effects and free carriers are generated solely due to the pump and not due to the weaker probe. The rate equations for the energy normalized pump and probe amplitudes a_r^{pump} and a_r^{probe} in the MRR can be derived by substituting $j(\omega - \omega_{\text{pump}}) \to \frac{d}{dt}$ and $j(\omega - \omega_{\text{probe}}) \to \frac{d}{dt}$, respectively and $\tilde{\omega}_o = \omega_o + \Delta\omega_o^L + \Delta\omega_o^{NL} + j \left(r_o + \Delta r_o^L + \Delta r_o^{NL} \right)$. The equations for all-pass (1 × 1) MRR configuration can be modified to account for the additional drop waveguide for add-drop (1 × 2) geometry and are given by

$$\frac{d}{dt} a_r^{\text{pump}}(t)$$
$$= -j \left[\omega_{\text{pump}} - \omega_o - \Delta\omega_o^L(t) - \Delta\omega_o^{NL}(t) \right] a_r^{\text{pump}}(t)$$
$$- \left[r_o + \Delta r_o^L(t) + \Delta r_o^{NL}(t) \right] a_r^{\text{pump}}(t)$$
$$- (r_e + r_d) a_r^{\text{pump}}(t) - j\sqrt{2r_e} A_i^{\text{pump}}(t) \tag{10a}$$

$$\frac{d}{dt} a_r^{\text{probe}}(t)$$
$$= -j \left[\omega_{\text{pump}} - \omega_o - \Delta\omega_o^L(t) - \Delta\omega_o^{NL}(t) \right] a_r^{\text{probe}}(t)$$
$$- \left[r_o + \Delta r_o^L(t) + \Delta r_o^{NL}(t) \right] a_r^{\text{probe}}(t)$$
$$- (r_e + r_d) a_r^{\text{probe}}(t) - j\sqrt{2r_e} A_i^{\text{probe}}(t). \tag{10b}$$

To calculate the complex resonance frequency and the transient response, (10) is numerically integrated with (6)–(9). The transmitted probe amplitudes at P_t and P_d can be deduced by substituting (10b) in (3) and (4) and plotted using (5). The same relations can be assumed when $A_a \neq 0$ at P_a, due to symmetry resulting in a 2 × 2 switch with a single MRR. The rate of change in energy for probe can then be given by

$$\frac{da_r}{dt} = \left(j\omega_o - \frac{1}{\tau} \right) a_r - j\mu_e A_i - j\mu_d A_a \tag{11}$$

and the output field amplitudes in the waveguide as

$$A_t(t) = A_i(t) - 2j\sqrt{2r_e} a_r(t) \tag{12}$$

$$A_d(t) = A_a(t) - 2j\sqrt{2r_d} a_r(t) \tag{13}$$

III. RESULTS AND DISCUSSION

The optical switching characteristics, namely the variation in the normalized probe transmission with time for a 1 × 2 silicon MRR have been computed by solving equations (3)–(10) through computer simulations considering the experimental data, i.e. $R = 100 \mu$m, $A = 450$ nm × 250 nm,
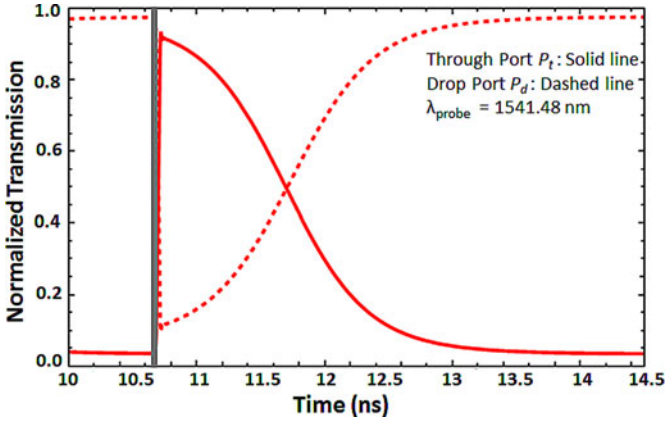
Fig. 2. Variation of normalized transmission of probe with time in silicon MRR 1×2 add-drop configuration using experimental parameters [11]. The pump pulse is indicated in grey.

$\lambda_{\mathrm{probe}} = 1541.48$ nm, $\lambda_{\mathrm{pump}} = 415$ nm, $Q = 19000$, $\tau_{fc} = 450$ ps, and $E_{\mathrm{pump}} = 3.2$ pJ at critical coupling condition [11]. In the experiment, Dong *et al.* have demonstrated comb switching by injecting a *cw* probe (λ_{probe})along with a femtosecond pulsed pump(λ_{pump})into a MRR. When the pump is incident on the ring, carriers are generated within the ring waveguide due to which the probe is directed to P_t. As the free carriers recombine, resonance of the ring is restored and the input is now retransmitted to P_d. This is also evident from the simulated temporal response that shows the initial *ps* increase in normalized transmission at P_t and the complementary decrease at P_d followed by a gradual decrease and increase in transmission in *ns* at P_t and P_d respectively (see Fig. 2). The rise time obtained in the simulations is 15 ps and fall time is 920 ps. The measured response of the MRR switch demonstrates 20% - 80% rise and fall times of 100 ps and 0.93 ns, respectively, according to experimental results. However, the measured rise time is detector-limited, and is theoretically expected to be only 15 ps. Fig. 2 shows that the theoretical simulations are in extremely good agreement with reported experimental results [11].

In order to design logic circuits with a smaller footprint, we consider a silicon 2×2 add-drop MRR optimally coupled to the waveguides. We have considered values for the various parameters listed in Table I from multiple experiments [8], [9], [22], [29] and optimized the values of reported Q, pump-probe delay and P_c for low-power ultrafast and high contrast switching. Considering the coupling conditions, the computed values of power coupling coefficients ($\kappa_e = \kappa_d$) is $\cong 0.2$. Switching time is limited by the ring charging time and the recombination time of the induced carriers and usually depends on the carrier lifetime as it is generally longer than the cavity photon lifetime. To increase the bit rate and speed of operation, the free-carrier dynamics during injection and extraction can be controlled inside the MRR by a combination of several distinct mechanisms [29].

The average input control power (P_c) required for modulation is given by $P_c^2 \geq \frac{\pi^2 n_g^2 n_{\mathrm{eff}} h \nu_c V_{\mathrm{eff}}^2}{2\Gamma n_f \beta \lambda_2^2 Q_2^2 Q_1 \tau_{fc}}$ where n_f is the ratio between refractive index change and carrier density, n_{eff} is effective index of the ring waveguide and $h\nu_c$is control photon energy [9]. As P_c is inversely proportional to τ_{fc} and Q, we have considered the reported experimental value of $Q = 11,076$ [8], such that

TABLE I
PARAMETERS USED IN THE SIMULATIONS [8], [9], [22], [29]

Radius (R)	5µm
Rectangular cross-section (A)	450 x 250 nm
λ_{pump} (λ_{res1})	1550.55 nm
Q_{res1} ($\lambda_{\mathrm{res1}}/\Delta\lambda_{\mathrm{FWHM1}}$)	11076
$\Delta\lambda_{\mathrm{FWHM1}}$	0.14 nm
$\tau_{\mathrm{cav1}}(\lambda_{\mathrm{res1}}^2/2\pi c\Delta\lambda_{\mathrm{FWHM1}})$	9.1 ps
λ_{probe} (λ_{res2})	1568.55 nm
$Q_{\mathrm{res2}}(\lambda_{\mathrm{res2}}/\Delta\lambda_{\mathrm{FWHM2}})$	9804
$\Delta\lambda_{\mathrm{FWHM2}}$	0.16 nm
$\tau_{\mathrm{cav2}}(\lambda_{\mathrm{res2}}^2/2\pi c\Delta\lambda_{\mathrm{FWHM2}})$	8.1 ps
Free-carrier lifetime (τ_{fc})	15 ps
Pump pulse width	0.1 ps
Probe pulse width	18 ps
Pump-probe delay	6 ps
$P_c(E_{pump})$	~ 25 mW (~ 2.6 pJ)
FSR = λ_o^2 / Ln_g	18 nm
Group index (n_g)	4.35
Γ	0.92
n_r	3.48
A/A_{eff}	0.82
β	0.79 cm/GW
n_{21}	0.45 x 10⁻¹³ cm²/W

$P_c = 25$ mW, switch-on/off is 9 ps/25 ps and the modulation is 85%. The switching characteristics are sensitive to P_c. Increasing P_c leads to increase in switching contrast and switch-off time due to increase in TPA-induced free carriers, whereas the switch-on time decreases. For instance, for $P_c = 21$, 29 and 51 mW, the contrast is 50%, 94% and 100%, switch-off time is 14, 35 and 80 ps and switch-on time is 12, 4 and 1 ps respectively. P_c can be reduced by considering a lower contrast.There is a trade-off between P_c and switching time. For the highest Q-factor reported for a silicon MRR $\sim 2.2 \times 10^7$ [30], $P_c \sim 13$ µW resulting in a switch-on time of 15 ns. On the other hand, increasing τ_{fc} to 500 ps, P_c is ~4.9 mW with 85% modulation. Alternatively, the ring size can also be reduced to lower P_c. TPA (β) decreases with increase in wavelength between 800–2000 nm, although it is nearly constant between 1500–1700 nm [31]. Increasing β to 1 cm/GW leads to $P_c = 23.3$ mW for the same switching response.

To estimate practical power values involved in the logic operations, we consider the experimental conditions of Xu *et al.* with a probe laser of 5 mW, of which $\sim$30% (1.5 mW) gets coupled through a nano-tapered waveguide [10]. At off-resonance $\sim$92% (1.4 mW) and at resonance only $\sim$15% (0.2 mW) of it gets coupled from P_i to P_t or from P_a to P_d [9], [10]. We assume 18% of the pump ($\sim$8 dB loss due to coupling, scattering and absorption) i.e. $\sim$4.5mW is detected from the MRR [32]. We also consider positive logic and an upper limit of low-state output power $P_{\mathrm{OL}} = 0.3$ mW (maximum value for logic 0) and minimum threshold for the high-state output power $P_{\mathrm{OH}} = 0.9$ mW (minimum value for logic 1) for the probe output, to realize various logic operations. Considering the inputs as pump and probe intensities, the all-optical silicon MRR switch (see Fig. 1) is used as a building block for designing higher computing circuits and the temporal response i.e. the variation in normalized power transmission (NPT) with time has been simulated by solving equations (3)–(10) using the experimental parameters in Table I.
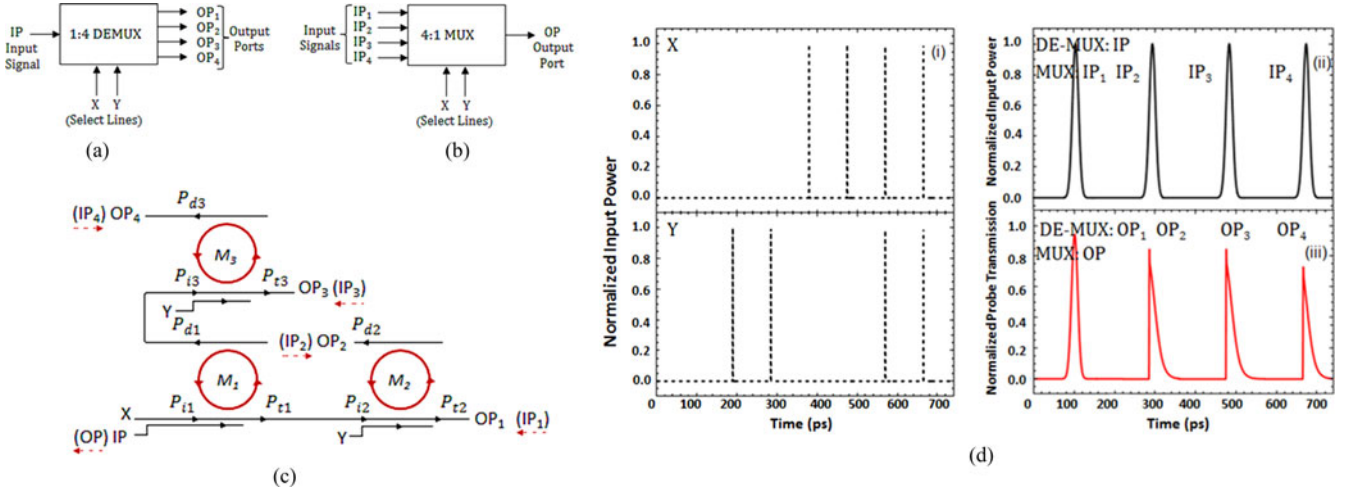
Fig. 3. (a) Block Diagram of 1:4 DEMUX, (b) Block Diagram of 4:1 MUX, (c) Schematic of all-optical DEMUX/MUX, (d) Variation of normalized input power and probe transmission with time: (i) Pump inputs (dashed), (ii) Probe inputs, (iii) Probe outputs.

TABLE II
TRUTH TABLE FOR ALL-OPTICAL 4:1 DEMUX AND 1:4 MUX

Select Lines		DEMUX Input	DEMUX Outputs				MUX Inputs				MUX Output
X(mW)	Y(mW)	IP(mW)	OP_1(mW)	OP_2(mW)	OP_3(mW)	OP_4(mW)	IP_1(mW)	IP_2(mW)	IP_3(mW)	IP_4(mW)	OP(mW)
0	0	0	0	X	X	X	0	X	X	X	0
0	0	1 (1.5)	1 (1.4)	X	X	X	1 (1.5)	X	X	X	1 (1.4)
0	1 (25)	0	X	0	X	X	X	0	X	X	0
0	1 (25)	1 (1.5)	X	1 (1.3)	X	X	X	1 (1.5)	X	X	1 (1.3)
1 (25)	0	0	X	X	0	X	X	X	0	X	0
1 (25)	0	1 (1.5)	X	X	1 (1.3)	X	X	X	1 (1.5)	X	1 (1.3)
1 (25)	1 (25)	0	X	X	X	0	X	X	X	0	0
1 (25)	1 (25)	1 (1.5)	X	X	X	1 (1.1)	X	X	X	1 (1.5)	1 (1.1)

A. All-Optical DEMUX/MUX

A DEMUX is a fundamental combinatorial and function generator circuit used to de-multiplex an input signal (*IP*) from an input channel to one of the many output channels (OP_1–OP_4) whereas, a MUX is used to multiplex inputs (IP_1–IP_4) from a number of input channels to a single output channel (OP) depending on the select lines X and Y.

Figs. 3(a) and (b) show the block diagrams of 1:4 DEMUX and 4:1 MUX respectively. Fig. 3(c) shows the architecture of a DEMUX/MUX and Fig. 3(d) shows the simulated response. Pump inputs are considered as X and Y select lines at λ_{pump} and are coupled along with a probe input at λ_{probe} into the MRRs as shown. X and Y inputs in the simulations are also as shown in Fig. 3(d-i), the normalized input power of probe (IP) coupled at P_{i1} of M_1 in Fig. 3(d-ii) and the OPs in terms of the NPT in Fig. 3(d-iii). The different combinations of X, Y and IP result in the realization of the DEMUX/MUX operations (Truth Table II). Case (i): X = Y = IP = 0: no light is detected in any of the output ports. Case (ii): X = Y = 0, IP = 1: MRR switches are in the off-resonant state, IP passes from P_{i1} to P_{t2} resulting in $OP_1 = 1$, corresponding to the simulated NPT $\sim 92\%$ at 100 ps in Fig. 3(d-iii). Case (iii): X = 0, Y = 1, IP = 0: no output is detected. Case (iv): X = 0, Y = IP = 1: P_{i1} gets switched by M_2 to P_{d2} resulting in $OP_2 = 1$. This corresponds to the simulated NPT $\sim 85\%$ at 290 ps [see Fig. 3(d-iii)]. Case (v): X = 1, Y = IP = 0: although M_1 is on-resonance, no output

is detected. Case (vi): X = 1, Y = 0, IP = 1: IP is switched to P_{d1} by M_1 to emerge at P_{t3} to result in $OP_3 = 1$ that corresponds to NPT $\sim 85\%$ at 480 ps [see Fig. 3(d-iii)]. Case (vii): X = Y = 1, IP = 0: M_1, M_2 and M_3 are in the on-resonant state. However, no output is detected. Case (viii): X = Y = IP = 1: IP is switched from P_{i1} to P_{d1} by M_1 and further switched to P_{d3} by M_3. This corresponds to $OP_4 = 1$ as shown by the simulated signal at 670 ps (NPT $\sim 72\%$) in Fig. 3(d-iii). The same DEMUX configuration can also be used to realize a 4:1 MUX which is shown in Fig. 3(c) with dashed lines. In this case, the inputs IP_1 to IP_4 are incident on switches M_1 and M_2 and based on the different combinations of X and Y, one of the inputs gets switched to result in OP = 1. Now, Fig. 3(d-ii) conforms to the inputs ($IP_1 - IP_4$) at different ports and Fig. 3(d-iii) to the output (OP). The corresponding truth table for 4:1 MUX is also shown in Table II. Three switches are required for 1:4 DEMUX or 4:1 MUX operation, the architecture can also be expanded to multiplex n number of lines, for which 2n-1 switches would be required.

B. All-Optical Fredkin Gate

Fig. 4(a) shows the schematic of a three-input and three-output Fredkin logic gate. The truth table is shown in Table III and Fig. 4(b) shows the simulated response of the proposed Fredkin gate. The pump I_1 (dashed lines) and probe inputs I_2
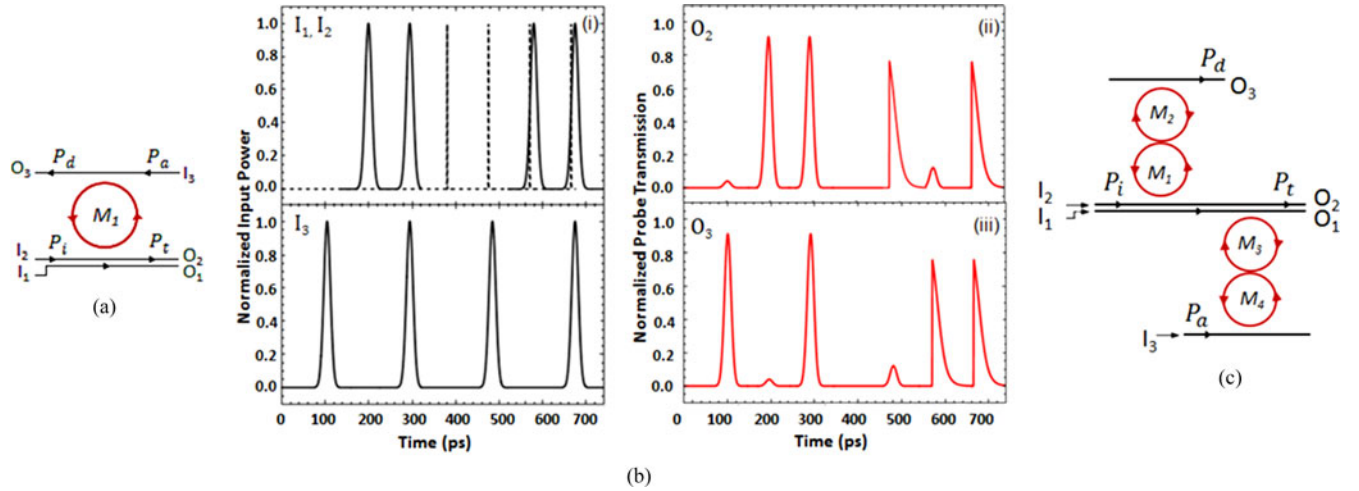
Fig. 4.   (a) Schematic of the all-optical Fredkin gate, (b) Variation of normalized input power and probe transmission with time: (i) Pump input (dashed), Probe inputs (solid), (ii) Probe output O_2, (iii) Probe output O_3. (c) Alternative implementation using double-stage second-order add-drop configuration.

(solid lines) are shown in Fig. 4(b-i). I_1 and I_2 are coupled at P_i whereas I_3 is coupled at P_a of M_1 [see Fig. 4(a)]. When $I_1 = 0$, I_2 and I_3 pass to P_t and P_d respectively. However, when $I_1 = 1$, M_1 switches I_2 and I_3 from P_i and P_a to P_d and P_t respectively. Fredkin gate maps out one input to one output, this can be implemented with I_1 mapping out to O_1. Case (i): $I_1 = I_2 = I_3 = 0$: no output is detected. Case (ii): $I_1 = I_2 = 0, I_3 = 1$: I_3 passes to P_d resulting in $O_3 = 1$, corresponding to the simulated NPT $\sim 92\%$ at 100 ps as shown in Fig. 4(b-iii). Case (iii): $I_1 = 0, I_2 = 1, I_3 = 0$: $O_2 = 1$ as I_2 passes from P_i to P_t (simulated NPT at 200 ps). Case (iv): $I_1 = 0, I_2 = I_3 = 1$: $O_2 = O_3 = 1$ at 290ps as both I_2 and I_3 pass from P_i and P_a to P_t and P_d respectively. Case (v): $I_1 = 1, I_2 = I_3 = 0$: no output is detected. Case (vi): $I_1 = 1, I_2 = 0, I_3 = 1$: M_1 switches I_3 from P_a to P_t, resulting in $O_2 = 1$ corresponding to the simulated NPT $\sim 85\%$ at 480 ps [see Fig. 4(b-ii)]. Case (vii): $I_1 = I_2 = 1, I_3 = 0$: I_2 is switched from P_i to P_d, resulting in $O_3 = 1$ obtained at 575 ps [see Fig. 4(b-iii)]. Case (viii): $I_1 = I_2 = I_3 = 1$: I_2 gets switched from P_i to P_d and I_3 gets switched from P_a to P_t, resulting in $O_2 = O_3 = 1$ [simulated NPT at 670 ps in Fig. 4(b-ii) and Fig. 4(b-iii)].The probe output at 200 ps is in the absence of the pump pulse. The rise-time of the peak at 480 ps is smaller than that at 200 ps due to the pump pulse that triggers the generation of free carriers 6 ps earlier than the peak probe pulse. The various input and output combinations result in the implementation of the Fredkin logic gate as shown in Fig. 4 and in Truth Table III.

In the case of Fredkin gate, the relative phase between the two probe inputs of the same wavelength may induce intraband crosstalk. It has been experimentally shown that when input signals of the same wavelengths are simultaneously given at P_t and P_d, crosstalk increases as the frequency difference between the two signals increases [33]. Thus, coherent input signals from the same laser source at both the ports are given simultaneously to avoid any frequency mismatch. A high coupling strength $(\kappa_e = \kappa_d \cong 0.85)$ can be considered in the designs to minimize crosstalk [33]. It has also been shown that the use of an active

TABLE III
TRUTH TABLE FOR ALL-OPTICAL FREDKIN GATE

Pump Input	Probe Inputs		Fredkin gate Outputs		
I_1(mW)	I_2(mW)	I_3(mW)	O_1(mW)	O_2(mW)	O_3(mW)
0	0	0	0	0	0
0	0	1 (1.5)	0	0 (0.1)	1 (1.4)
0	1 (1.5)	0	0	1 (1.4)	0 (0.1)
0	1 (1.5)	1 (1.5)	0	1 (1.4)	1 (1.4)
1 (25)	0	0	1 (4.5)	0	0
1 (25)	0	1 (1.5)	1 (4.5)	1 (1.3)	0 (0.2)
1 (25)	1 (1.5)	0	1 (4.5)	0 (0.2)	1 (1.3)
1 (25)	1 (1.5)	1 (1.5)	1 (4.5)	1 (1.3)	1 (1.3)

ring resonator provides complete loss compensation and can be used to eliminate the crosstalk [33]. Alternatively, crosstalk can also be minimized by implementing the proposed circuits with a single MRR replaced by a double-stage configuration, where the drop operation is performed separately on the first stage while the add input is given on the second stage [33]. An alternate design of Fredkin gate is shown in Fig. 4(c) although it requires 4 MRRs and increases the complexity, switching time, size and cost of the circuit. Two probes at different wavelengths can also be used. The relative phase between them will induce interband cross-talk which can be easily removed by a filter.

C. All-Optical Toffoli Gate

The Toffoli gate is a universal reversible logic gate, which is also known as the "controlled-controlled-not" gate. It has a 3 bit input and output, and if the first two bits are set, it flips the third bit, as shown in Truth Table IV. It can also be described as mapping bits I_1, I_2 and I_3 to I_1, I_2 and I_3 XOR $(I_1$ AND $I_2)$. The design of an all-optical Toffoli gate is shown in Fig. 5(a). Fig. 5(b) shows the simulated response of the Toffoli gate operation. We consider two pump inputs I_1 and I_2 at λ_{pump} shown in Fig. 5(a) and also in Fig. 5(b-i) as dashed lines. The probe input I_3 at λ_{probe} [see Fig. 5(b-ii)] is given at P_{i1} and
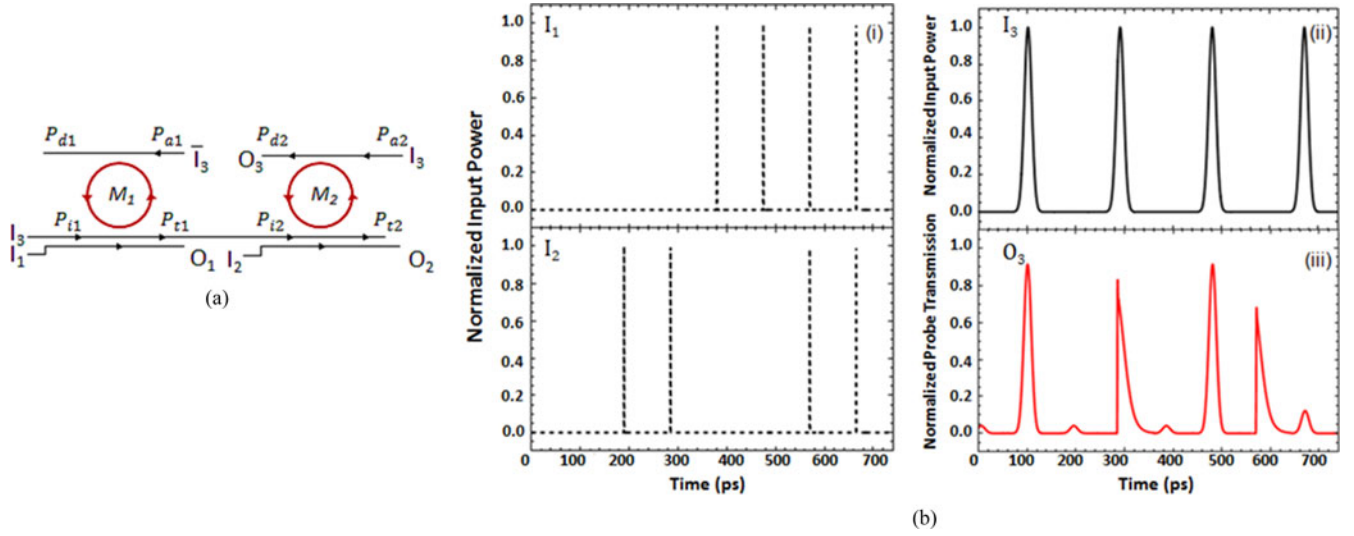
Fig. 5. (a) Schematic of the all-optical Toffoli gate, (b) Variation of normalized input power and probe transmission with time: (i) Pump inputs (dashed), (ii) Probe inputs, (iii) Probe output O_3.

TABLE IV
TRUTH TABLE FOR ALL-OPTICAL TOFFOLI GATE

Pump Inputs			Probe Input	Toffoli Gate Outputs		
I_1 (mW)	I_2 (mW)	I_3 (mW)	I_3 (mW)	O_1 (mW)	O_2 (mW)	O_3 (mW)
0	0	0		0	0	0 (0.1)
0	0	1 (1.5)		0	0	1 (1.4)
0	1 (25)	0		0	1 (4.5)	0 (0.1)
0	1 (25)	1 (1.5)		0	1 (4.5)	1 (1.3)
1 (25)	0	0		1 (4.5)	0	0 (0.1)
1 (25)	0	1 (1.5)		1 (4.5)	0	1 (1.4)
1 (25)	1 (25)	0		1 (4.5)	1 (4.5)	1 (1.1)
1 (25)	1 (25)	1 (1.5)		1 (4.5)	1 (4.5)	0 (0.2)

P_{a2} whereas $\overline{I_3}$ is the input at P_{a1}. This can be implemented by either two laser diodes or by a single diode with an inverter [see Fig. 5(a)]. Toffoli gate maps two inputs to two outputs, that are implemented with I_1 and I_2 mapping to O_1 and O_2 respectively. The various input and output combinations result in the implementation of the Toffoli logic gate as shown in Fig. 5 and in Table IV.

A double-stage implementation is not required for Toffoli and MUX/DEMUX logic operations as they don't require simultaneous probe inputs. It is important to control the relative phase between the probe pulses and also the probe and pump for cascadability. It can be minimized by ensuring equal path lengths for the two probe inputs into the MRR and also when cascading, as shown in the designs of various Fredkin-based all-optical computing circuits [25]. Appropriate phase delays can be incorporated in the circuits and the pump duration can also be increased to avoid pump-probe delays. In our simulations, a pump-probe delay of 6 ps has been considered i.e., the pump is incident 6 ps before the probe peak to achieve a high switching contrast (85%). A delay of 7 and 13 ps reduces contrast to 82% and 50% respectively. Reducing the delay to 4 and 0 ps, leads to a contrast of 86% and 90% respectively. However, it results

in a high probe transmission (34% and 62% respectively) to an undesired port.

MRRs are compact, can be actuated directly as a lumped element at high speeds (10–25 GHz) and hold the best potential in terms of modulation energy per bit [4].In the proposed designs, the control and probe both are considered as logical inputs, instead of either the control or probe signals as in earlier designs,thereby reducing the number of switches and inputs to the circuit that would result in lower delays and higher bit rates [6], [7], [14]. DEMUX/MUX operations require only three switches and can be realized from the same circuit by interchanging the inputs and outputs. Since the state of each switch is controlled by an input logic signal, all switches operate simultaneously and the switching time does not accumulate. Fredkin gate has been implemented using one switch and Toffoli requires two switches only, thus, reducing both delay and complexity of the circuit. The pump-probe technique can be used advantageously to cascade the gates to realize higher arithmetic and logic circuits. For instance, the proposed universal all-optical Fredkin logic gate can be used to realize all-optical full-adder, MUX/DEMUX, XOR/XNOR as has been shown with BR-coated silica microcavities, by cascading the pump and the probe outputs at P_t and P_d as inputs to other logic gates [25]. Also, the pump and probe wavelengths can be interchanged as shown experimentally in [8], [9], which provides additional flexibility in cascading. For instance, in the design of a T flip-flop [34].

Advantages of BDD/DL, reconfigurability, tunability, high fan-out, simplicity and flexibility of cascading switches in 2D architectures for large-scale integration make the proposed designs promising for practical applications. They require less number of switches and inputs for realization of the desired logic compared to earlier reported designs and to the best of our knowledge are the first implementations of all-optical ultrafast reversible logic with CMOS-compatible silicon MRRs.

REFERENCES

[1] B. Jalali and S. Fathpour, "Silicon photonics," *J. Lightw. Technol.*, vol. 24, no. 12, pp. 4600–4615, Dec. 2006.

[2] M. Lipson, "Guiding, modulating, and emitting light on silicon-challenges and opportunities," *J. Lightw. Technol.*, vol. 23, no. 12, pp. 4222–4238, Dec. 2005.

[3] G. T. Reed, G. Mashanovich, F. Y. Gardes, and D. J. Thomson, "Silicon optical modulators," *Nature Photon.*, vol. 4, no. 8, pp. 518–526, Aug. 2010.

[4] W. Bogaerts, P. D. Heyn, T. V. Vaerenbergh, K. D. Vos, S. K. Selvaraja, T. Claes, P. Dumon, P. Bienstman, D. V. Thourhout, and R. Baets, "Silicon microring resonators," *Laser Photon. Rev.*, vol. 6, no. 1, pp. 47–73, Jan. 2012.

[5] T. Y. and X. Cai, "On power consumption of silicon microring based optical modulators," *J. Lightw. Technol.*, vol. 28, no. 11, pp. 1615–1623, Jun. 2011.

[6] Q. Xu and R. Soref, "Reconfigurable optical directed logic circuits using microresonator-based optical switches," *Opt. Exp.*, vol. 19, no. 6, pp. 5244–5259, Mar. 2011.

[7] Y. H. Tian, L. Zhang, R. Q. Ji, L. Yang, P. Zhou, H. T. Chen, J. F. Ding, W. W. Zhu, Y. Y. Lu, L. X. Jia, Q. Fang, and M. B. Yu, "Proof of concept of directed OR/NOR and AND/NAND logic circuit consisting of two parallel microring resonators," *Opt. Lett.*, vol. 36, no. 9, pp. 1650–1652, May 2011.

[8] Q. Xu and M. Lipson, "All-optical logic based on silicon micro-ring resonators," *Opt. Exp.*, vol. 15, no. 3, pp. 924–929, Jan. 2007.

[9] Q. Xu, V. R. Almeida, and M. Lipson, "Micrometer-scale all-optical wavelength converter on silicon," *Opt. Lett.*, vol. 30, no. 20, pp. 2733–2735, Oct. 2005.

[10] S. F. Preble, Q. Xu, and M. Lipson, "Changing the color of light in a silicon resonator," *Nature Photon.*, vol. 1, no. 5, pp. 293–296, May 2007.

[11] P. Dong, S. F. Preble, and M. Lipson, "All-optical compact silicon comb switch," *Opt. Exp.*, vol. 15, no. 15, pp. 9600–9605, Jul. 2007.

[12] S. Lin, Y. Ishikawa, and K. Wada, "Demonstration of optical computing logics based on binary decision diagram," *Opt. Exp.*, vol. 20, no. 2, pp. 1378–1384, Jan. 2012.

[13] S. Roy and M. Prasad, "Design of all-optical reconfigurable logic unit with bacteriorhodopsin protein coated microcavity switches," *IEEE Trans. Nanobiosci.*, vol. 10, no. 3, pp. 160–171, Sep. 2011.

[14] H. J. Caulfield, R. A. Soref, and C. S. Vikram, "Universal reconfigurable optical logic with silicon-on-insulator resonant structures," *Photon. Nanostruct.*, vol. 5, no. 1, pp. 14–20, Oct. 2007.

[15] Y.-P. Huang and P. Kumar, "Interaction-free quantum optical Fredkin gates in χ^2 microdisks," *IEEE J. Quantum Electron.*, vol. 18, no. 2, pp. 600–611, Apr. 2012.

[16] H.-R. Wei and F.-G. Deng, "Universal quantum gates for hybrid systems assisted by quantum dots inside double-sided optical microcavities," *Phys. Rev. A*, vol. 87, no. 2, pp. 022305–022315, Feb. 2013.

[17] M. Z. Zhu and X. G. Yin, "Highly efficient optical fredkin gate with weak nonlinearities and classical information feed-forward," *J. Opt. Soc. Amer. B*, vol. 30, no. 2, pp. 355–361, Feb. 2013.

[18] R. Orbach, F. Remacle, R. D. Levine, and I. Willner, "Logic reversibility and thermodynamic irreversibility demonstrated by DNAzyme-based toffoli and fredkin logic gates," *Proc. Nat. Acad. Sci.*, vol. 109, no. 52, pp. 21228–21233, Dec. 2012.

[19] V. M. Stojanović, A. Fedorov, A. Wallraff, and C. Bruder, "Quantum-control approach to realizing a Toffoli gate in circuit QED," *Phys. Rev. B*, vol. 85, no. 5, pp. 054504–054507, Feb. 2012.

[20] A. Fedorov, L. Steffen, M. Baur, M. P. da Silva, and A. Wallraff, "Implementation of a Toffoli gate with superconducting circuits," *Nature*, vol. 481, no. 7380, pp. 170–172, Dec. 2011.

[21] J. Cody, "Low-overhead constructions for the fault-tolerant Toffoli gate," *Phys. Rev. A*, vol. 87, no. 2, pp. 022328–022331, Feb. 2013.

[22] C. Manolatou and M. Lipson, "All-optical silicon modulators based on carrier injection by two-photon absorption," *J. Lightw. Technol.*, vol. 24, no. 3, pp. 1433–1439, Mar. 2006.

[23] C. Li and D. Na, "Optical switching in silicon nanowaveguide ring resonators based on kerr effect and TPA effect," *Chin. Phys. Lett.*, vol. 20, no. 5, pp. 0542031–0542033, Nov. 2009.

[24] S. Roy, M. Prasad, J. Topolancik, and F. Vollmer, "All-optical switching with bacteriorhodopsin protein coated microcavities and its application to low power computing circuits," *J. Appl. Phys.*, vol. 107, no. 5, pp. 053115–053124, Mar. 2010.

[25] S. Roy and M. Prasad, "Novel proposal for all-optical Fredkin logic gate with bacteriorhodopsin-coated microcavity and its applications," *Opt. Eng.*, vol. 49, no. 6, pp. 065201–065210, Jun. 2010.

[26] S. Roy, P. Sethi, J. Topolancik, and F. Vollmer, "All-optical reversible logic gates with optically controlled bacteriorhodopsin protein-coated microresonators," *Adv. Opt. Technol.*, vol. 2012, pp. 727206–727212, Jun. 2012.

[27] B. E. Little, S.-T. T. Chu, H. A. Haus, J. S. Foresi, and J.-P. P. Laine, "Microring resonator channel dropping filters," *J. Lightw. Technol.*, vol. 15, no. 6, pp. 998–1005, Jun. 1997.

[28] M. Dasic and M. A. Popovic, "Minimum drop-loss design of microphotonic microring-resonator channel add-drop filters," in *Proc. Telecommun. Forum*, Nov. 2012, vol. 20, pp. 927–930.

[29] M. Waldow, T. Plötzing, M. Gottheil, M. Först, J. Bolten, T. Wahlbrink, and H. Kurz, "25ps all-optical switching in oxygen implanted silicon-on-insulator microring resonator," *Opt. Exp.*, vol. 16, no. 11, pp. 7693–7702, May 2008.

[30] A. Biberman, M. J. Shaw, E. Timurdogan, J. B. Wright, and M. R. Watts, "Ultralow-loss silicon ring resonators," in *Proc. IEEE 9th Int. Conf. Group IV Photon.*, 2012, pp. 39–41.

[31] A. D. Bristow, N. Rotenberg, and H. M. Van Driel, "Two-photon absorption and Kerr coefficients of silicon for 850–2200," *Appl. Phys. Lett.*, vol. 90, no. 19, pp. 191104–191104, May 2007.

[32] A. C. Turner, M. A. Foster, A. L. Gaeta, and M. Lipson, "Ultra-low power parametric frequency conversion in a silicon microring resonator," *Opt. Exp.*, vol. 16, no. 7, pp. 4881–4887, Mar. 2008.

[33] H. Simos, C. Mesaritakis, D. Alexandropoulos, and D. Syvridis, "Dynamic analysis of crosstalk performance in microring-based add/drop filters," *J. Lightw. Technol.*, vol. 27, no. 12, pp. 2027–2034, Jun. 2009.

[34] P. Sethi and S. Roy, "Ultrafast all-optical flip-flops, simultaneous comparator-decoder and reconfigurable logic unit with silicon microring resonator switches," *IEEE J. Sel. Topics Quantum Electron.*, vol. 20, no. 4, Jul.-Aug. 2014, in press.

Purnima Sethi received the B.Sc. (Hons.) degree in physics, the M.Sc. degree in physics with specialization in electronics and the M.Phil. degree, in 2008, 2010, and 2011, respectively, all from Dayalbagh Educational Institute, Agra, India, where she is currently working toward the Ph.D. degree in the Department of Physics and Computer Science.

Her research interests include nanobiophotonics, biomolecular computing, and silicon photonics.

Ms. Sethi received the Director's medal for securing highest marks in M.Phil. (Physics) and the Best Paper Award at the IEEE Workshop on Recent Advances in Photonics held at IIT Delhi in Dec. 2013.

Sukhdev Roy received the B.Sc. (Hons.) degree in physics from Delhi University, Delhi, India, and the M.Sc. in physics with specialization in electronic science from Dayalbagh Educational Institute, Agra, India, in 1986 and 1988, respectively. He received the Ph.D. degree in physics from the Indian Institute of Technology Delhi, India, in 1993.

He joined the Department of Physics and Computer Science, Dayalbagh Educational Institute, Agra, India, where he is currently a Professor. He has been a Visiting Scientist at Harvard University, University of Waterloo, Osaka University, Hokkaido University, City University, London, Queen Mary University of London, Tata Institute of Fundamental Research, Mumbai, and the Indian Institute of Science, Bangalore. He is an Associate of the Abdus Salam International Centre for Theoretical Physics, Trieste, Italy. His current research interests include ultrafast all-optical information processing, energy conversion and sensing with natural photoreceptor proteins, organic molecules and silicon nanostructures.

Dr. Roy received a number of awards and fellowships that include the JSPS Invitation Fellowship, Japan, 2004, IETE Biennial Emerging Opto-electronic Technologies Award, 2012, 1st IETE B.B. Sen Memorial Award, 2007, Hari Om Ashram Prerit H.C. Shah Research Endowment Prize by Sardar Patel University, 2006, AICTE Career Award for Young Teachers, 2001 and many best paper awards. He was the Guest Editor of the March 2011 Special Issue of *IET Circuits, Devices* and *Systems Journal on Optical Computing*. He is a Fellow of the Indian National Academy of Engineering and Institution of Electronics and Telecommunication Engineers, India.